

**Department of Mathematics
Heidelberg University**

**An evaluation of mathematical models for stem cell
dynamics in neurogenesis**

Bachelor Thesis in Mathematics
submitted by

Maria Anita Stickel

2022

An evaluation of mathematical models for stem cell dynamics in neurogenesis

This Bachelor Thesis has been carried out by Maria Anita Stickel
at the Institute of Applied Mathematics in Heidelberg
under the supervision of
Prof. Dr. Anna Marciniak-Czochra
and
Dr. Diana-Patricia Danciu

Abstract. The dynamics of adult neurogenesis in the ventricular-subventricular zone are yet to be fully understood. In particular, how the pool of neural stem cells (NSCs), in active and quiescent states, is maintained while undergoing ageing effects. Mathematical modelling of biological systems can help to gain insight into such dynamics, to discover dependencies that may not be obvious purely from the data. This thesis evaluates different models of ordinary differential equations (ODEs) to describe those dynamics. First, a simplified, macroscopic model of neurogenesis based on an existing model of active and quiescent NSCs has been developed via a steady-state for the fraction of active NSCs among all NSCs. It was used to relate the parameters of the two former models via the macroscopic model, that does not inherently distinguish between active and quiescent cell states. Secondly, two neurogenesis model versions with constant and time-dependent self-renewal are compared and parameter estimation is applied to the macroscopic model. Although the NSC dynamics can be observed with all models, the macroscopic lense results in non-identifiable microscopic parameters. Furthermore, the model cannot capture the fraction of active NSCs among NSCs, as expected, due to the single equation it is defined by.

Zusammenfassung. Die Dynamik der adulten Neurogenese in der ventrikulär-subventrikulären Zone ist noch nicht vollständig geklärt. Insbesondere die Frage, wie die Population neuronaler Stammzellen (NSZs), in aktivem oder ruhendem Zustand, während der Alterung erhalten bleibt. Die mathematische Modellierung biologischer Systeme kann dazu beitragen, Einblicke in solche Dynamiken zu gewinnen und Abhängigkeiten zu entdecken, die aus den Daten allein nicht ersichtlich sind. In dieser Arbeit werden verschiedene Modelle gewöhnlicher Differentialgleichungen zur Beschreibung dieser Dynamik verglichen. Zunächst wurde ein vereinfachtes, makroskopisches Modell der Neurogenese auf der Grundlage eines bestehenden Modells aktiver und ruhender NSZ-Zustände entwickelt, das einen stationären Zustand für den Anteil der aktiven NSZ aus allen NSZ beschreibt. Es wurde verwendet um die Parameter der beiden früheren Modelle über das makroskopische Modell in Beziehung zu setzen, das von Natur aus nicht zwischen aktiven und ruhenden Zellzuständen unterscheidet. Zweitens werden zwei Neurogenesemodellversionen mit konstantem und zeitabhängigem Selbsterneuerungsparameter verglichen und Parameterschätzung wird auf das makroskopische Modell angewendet. Obwohl die NSZ-Dynamik mit allen Modellen beobachtet werden kann, führt die makroskopische Betrachtungsweise zu nicht identifizierbaren mikroskopischen Parametern. Darüber hinaus kann das Modell den Anteil der aktiven NSZ unter den NSZ nicht erfassen, wie erwartet, da es durch eine einzige Gleichung definiert ist.

Contents

1	Introduction	1
1.1	Mathematical modelling	1
1.2	Adult neurogenesis	1
1.3	Models	2
1.4	Goals of this thesis	2
2	The models	4
2.1	Active and quiescent cells	4
2.2	Total number of NSCs	5
3	Materials and methods	7
3.1	Solving ODEs	7
3.2	Parameter estimation	8
3.3	Model comparison	9
3.4	Experimental data	10
4	The fractions	11
4.1	The equilibrium points of $\frac{A}{Q+A}$	12
4.2	The convergence of $\frac{A}{Q+A}$	15
4.3	Application of the fraction results	16
5	Results	18
5.1	Comparing AaQNSC and TNSC model variations	18
5.2	Merged TNSC model	22
6	Final remarks	26

1 Introduction

1.1 Mathematical modelling

Mathematical biology is concerned with the development of mathematical models of biological systems, which, when combined with experimental data, can help to gain insight into complex processes, to discover underlying dynamics and dependencies that may not be obvious purely from the data. The use of Ordinary Differential Equations (ODEs) to model the change of system components over time is a common modelling approach, which can be used on different scales, from single molecule interactions up to describing whole organisms. It requires the assumption that the considered populations are well-mixed and that stochastic effects can be neglected, which is reasonable as large populations do not undergo rare statistical events. The equations result from the current understanding of the systems dynamics: the different components of the models in this study are neural stem cells (NSCs) in different activation stages (active NSCs (aNSCs) or quiescent NSCs (qNSCs)) and the main interactions are proliferation and transitions between those stages (differentiation and/or self-renewal). Given such a model, the parameters can be estimated numerically by fitting the model values to data. Furthermore, they enable us to observe how the systems dynamics depend on process parameters (such as rates or the initial state of the system) in a qualitative manner. Adding new plausible reactions or time-dependencies allows us to compare different model variations, taking into account complexity and capacity, to reflect the experimental observations. Moreover, it can provide guidance for future studies in order to confirm the hypothesized regulation terms and thus focus experimental efforts on the most important cases [9].

1.2 Adult neurogenesis

As most organs, the adult rodent brain has a population of multipotent stem cells that can replace tissue-specific cell types (like neurons or glia-cells) to face ageing or after injury. They have long-term self-renewal properties at an individual cell level and enable the generation of new neurons via differentiation, which is called neurogenesis. In the brain, this has been studied in two regions: the subgranular zone of the hippocampus and the ventricular-subventricular zone (V-SVZ) along the walls of the lateral ventricles, where the NSCs reside in niche structures [14]. In the V-SVZ mainly symmetric self-renewal and differentiation has been observed [16], yet the following models can capture asymmetric divisions, it is only the interpretation of the parameters that changes¹. The population of NSCs has been shown to be largely quiescent, with a time-declining fraction of cells who enter the cell cycle (are

¹The same holds for cell death, which is also not explicitly included in any of the following models.

activated) to either self-renew (two NSC clones arise from one NSC) or differentiate (two transit-amplifying progenitor cells arise from one NSC) [6]. Self-renewal maintains the stem cell pool of the adult organism in the niche, while further differentiated cells detach from the ventricle and migrate to the olfactory bulb [10, 11]. Whilst the stem cell pool declines with age, the numbers do not approach zero, suggesting that cells come out of quiescence to divide, and the daughter cells of self-renewal return to quiescence, limiting replication to avoid accumulation of mutations. Even after several rounds of symmetric self-renewal activated NSCs are able to return to long-term quiescence. The brain, like any other organ, is prone to ageing, which is accompanied by a continuous age-related cognitive decline, loss of regenerative capacity, limited plasticity, limited repair and reduced neurogenesis [8]. Additionally, trauma, seizures and diseases activate stem cell divisions, further contributing to the pool loss. To account for possible ageing-related effects observed in experimental data, time-dependent rates have been introduced. The most plausible mechanism explaining saturated decline with age is increasing quiescence, represented by declining activation. An alternative approach, which does not fit the data adequately is the increase of self-renewal of aNSCs, which leads to more NSCs instead of progenitors [23].

1.3 Models

The current study is based on the model presented by Kalamakis et al. (2019), where multiple scenarios for explaining the data from the V-SVZ are compared [10]. This model is adapted from the model of hippocampal neurogenesis introduced by Ziebell et al. (2014, 2018) [22, 23]. In turn, the models of Ziebell et al. (2014, 2018) are inspired from and use concepts introduced by the models for hematopoiesis by Stiehl et al. (2012, 2014) [20, 19]. In the model for hematopoiesis by Stiehl et al. (2012, 2014), only the total number of stem cells serves as a model component [20], while the model by Kalamakis et al. (2019) divides the cell population into two subgroups depending on their proliferation state (quiescent or active) [10].

1.4 Goals of this thesis

The first goal of this study is to develop a simplified, macroscopic model of neurogenesis starting from the existing model of Kalamakis et al. (2019) [10] and zooming out, pooling all types of NSCs into one compartment whose dynamics is governed by a macroscopic self-renewal rate as in the hematopoiesis models of Stiehl et al. (2012, 2014) [20, 19]. Two model versions, with constant and time-dependent self-renewal are compared. Secondly, an approximate model that merges the existing neurogenesis model by Kalamakis et al. (2019) with the macroscopic model introduced here via a steady-state of the constant Kalamakis et

al. (2019) model, is introduced and analysed in its ability to reproduce experimental data, and understand parameter relations and underlying mechanisms of neurogenesis.

2 The models

2.1 Active and quiescent cells

The following model of neurogenesis in the subventricular zone, which depicts the dynamics of neural stem cells, progenitor cells and neuroblasts as ODEs has been proposed by F. Ziebell [10]. It is based on the model of hematopoiesis by Stiehl et al. (2012) [20] and has been adapted by Ziebell et al. (2018) as a model of neurogenesis in the hippocampus [23]. With rate r , qNSCs are activated. aNSCs divide symmetrically with rate p , either into two quiescent stem cells (self-renewal) with probability b or into two progenitor cells (differentiation) with probability $(1 - b)$. In this second case, our model captures the exit of active stem cells from the system, whereas the behaviour of progenitor cells will not be covered in this thesis. This results in the following 2-dimensional linear system of ODEs:

$$\begin{aligned} \frac{d}{dt} \text{qNSC}(t) &= -r \cdot \text{qNSC}(t) + 2 \cdot b \cdot p \cdot \text{aNSC}(t) \\ \frac{d}{dt} \text{aNSC}(t) &= r \cdot \text{qNSC}(t) - p \cdot \text{aNSC}(t) \end{aligned} \quad (2.1)$$

Generic boundaries for r and b are $(0, 1)$ as they are probabilities, so overall we will study the following 2-dimensional linear system of ODEs:

$$\begin{aligned} \begin{pmatrix} \text{qNSC} \\ \text{aNSC} \end{pmatrix}' &= \begin{pmatrix} -r & 2bp \\ r & -p \end{pmatrix} \begin{pmatrix} \text{qNSC} \\ \text{aNSC} \end{pmatrix} \\ &\text{for } (r, b) \in (0, 1) \times (0, 1) \end{aligned} \quad (2.2)$$

The system has a unique solution which can be proven via the Picard-Lindelöf theorem [12], taking into account that finite linear matrix systems like (2.2) are always Lipschitz-continuous due to boundedness by the matrix norm. Age-related changes of cell numbers can be translated into time-dependent model parameters. Observed data shows a decline in the fraction $\frac{\text{aNSC}}{\text{NSC}} = \frac{\text{aNSC}}{\text{aNSC} + \text{qNSC}}$ which can be modeled with increasing quiescence through a time-decreasing activation rate of quiescent stem cells

$$r(t) = r_{max} \cdot e^{-\beta_r t}. \quad (2.3)$$

Another way which has been studied to be less effective [10] in incorporating this ageing effect is to substitute the constant parameter b with a time-dependent fraction of self-renewal

$$b(t) = \frac{1}{2}(1 + e^{-\beta_b t}(2 \cdot b_{min} - 1)) \quad (2.4)$$

describing an increase in self-renewal. The growth rate p will not be modified to model a time-dependent cell cycle (lengthening with age), as this was considered in [10], but could not explain the data. Proliferation rate p is derived from the average cell cycle length of neural stem cells measured by Ponti et al. (2013) to be $\tau^{stem} = 17.5\text{h}$ [17]. It is interpreted as the doubling time of the exponential growth process, leading to

$$p = \frac{\ln(2)}{\tau^{stem}}. \quad (2.5)$$

Any of the introduced time-dependent parameters still result in a unique solution via the Picard-Lindelöf theorem by additionally considering the finiteness of the functions of the incorporated changes ($r(t), b(t) \in (0, 1)$) and applying the matrix norm to the maximum.

Within the scope of this thesis this model will be referred to as the **AaQNSC** model (Figure 1a).

2.2 Total number of NSCs

An extension of the model to be introduced in this chapter has been studied in the case of hematopoiesis [20]. As shown in figure 1b, in our macroscopic neurogenesis model NSCs proliferate with rate p either through symmetric self-renewal (with probability a) leading to 2 NSC or through differentiation (probability $(1-a)$) resulting into 2 progenitor cells. In this second case our model captures the loss of one NSC, as the behaviour of progenitor cells will not be covered in this thesis. This is represented by the following differential equation

$$\begin{aligned} \frac{d}{dt} \text{NSC}(t) &= 2ap \text{NSC}(t) - p \text{NSC}(t) \\ &= (2a - 1)p \text{NSC}(t) \text{ for } a \in \left(0, \frac{1}{2}\right) \end{aligned} \quad (2.6)$$

where a indicates the ratio of self-renewal and has been shown to lie in $(0, \frac{1}{2})$ [20]. For a given initial value $\text{NSC}(0) = \text{NSC}_0$ this differential equation has a unique solution

$$\text{NSC}(t) = \text{NSC}_0 \cdot e^{(2a-1)pt} \quad (2.7)$$

An extension of this model, following the example of time-dependent self-renewal parameter $b(t)$ (2.4) from the AaQNSC model would be to introduce an increasing self-renewal rate

$$a(t) = \frac{1}{2}(1 + e^{\beta a t}(2 \cdot a_{min} - 1)). \quad (2.8)$$

Similarly to the AaQNSC model introduced above, any time-dependency of a still leads to a one-dimensional differential equation system with a unique solution due to the Picard-

Lindelöf theorem.

Within the scope of this thesis this model will be referred to as the **TNSC** model.

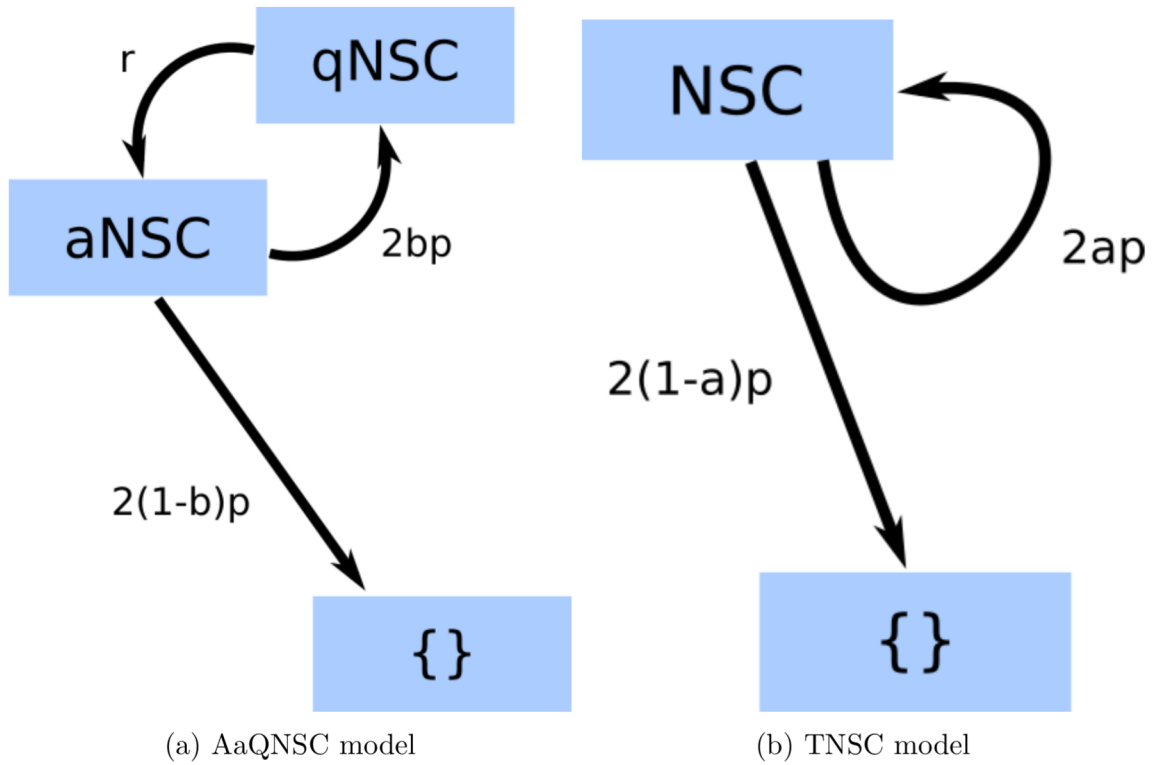


Figure 1: Schematic of the two neurogenesis models studied in this thesis

3 Materials and methods

3.1 Solving ODEs

For solving systems of differential equations in Matlab R2021a the routine ode45 has been used [13]. It is based on an explicit Runge-Kutta (4,5) formula, also called the Dormand-Prince pair [7]. It is a single-step solver which means that in each evaluation step $n \rightarrow n + 1$ the algorithm needs merely the value of the former step y_n and the former step-size h_n . Firstly, it computes the fourth and fifth order solutions of the Runge-Kutta method. The Runge-Kutta method includes the weighted increments m of several time points in the time interval $[t_n, t_{n+1}]$. The general formula for the fourth order Runge-Kutta with step-size h is

$$y_{n+1} = y_n + h \sum_{i=1}^4 b_i m_i$$

with increments

$$\begin{aligned} m_1 &= f(t_n, y_n) \\ m_2 &= f\left(t_n + \frac{h}{2}, y_n + m_1 \frac{h}{2}\right) \\ m_3 &= f\left(t_n + \frac{h}{2}, y_n + m_2 \frac{h}{2}\right) \\ m_4 &= f\left(t_n + \frac{h}{2}, y_n + m_3 \frac{h}{2}\right) \end{aligned}$$

such that the weights b_i satisfy

$$1 = \sum_{i=1}^4 b_i.$$

The difference between the fourth and fifth order Runge-Kutta calculations is used as the actual error of the fourth order solution in the determination of the adaptive step-size. This combined application of the Runge-Kutta methods makes the algorithm more time- and memory-efficient as it avoids unnecessary steps when the slope of the derivative changes little, but decreases the step size when the derivative changes a lot. In this implementation the default values of ode45's error tolerance and maximal number of function evaluations have been used.

3.2 Parameter estimation

To numerically fit parameters in a given model in such a way that they lead to NSC numbers closest to our observed data, an optimization problem had to be solved. As our model function is a solution of a system of ODEs and our parameters are in between certain boundaries to be biologically suitable, Matlab's `fmincon` Interior Point Algorithm for Constrained Optimization was used to estimate optimal parameters [18]. Given a problem

$$\min_x f(x) \text{ s. t. } c(x) \leq 0 \quad (3.1)$$

where x is the vector of parameters to be estimated, c are the boundaries and f is the objective function, the algorithm solves a sequence of approximate minimization problems

$$\min_{x,s} f_\mu(x, s) = \min_{x,s} f(x) - \mu \sum_i \log(s_i) \text{ s. t. } s \leq 0, g(x) + s = 0, l \in \mathbb{N}. \quad (3.2)$$

This version of (3.1) has an additional term to minimize a so-called logarithmic barrier function such that if the barrier parameter μ approaches zero, (3.2) approaches (3.1). There are two types of iteration steps. If possible², the algorithm takes a Direct step³ where (3.2) is optimized for the current given μ_l such that (x, s) gets adjusted. Otherwise the barrier parameter gets updated such that it further approaches 0. For the objective function, which quantifies the assumed error of a model, the standard approach is to use a least squares (LS) function:

$$\text{objective}_{LS} = \sum_{i=1}^n \varepsilon_i^2 \quad (3.3)$$

where

$$\varepsilon_i = y_i - g_j(x, t_i)$$

are the residuals, i.e. the distance between the measurements and the model values for different the models j at the same point in time. Instead of merely considering the squared residuals as in the general least squares (LS) method, a weighted least squares (WLS) approach was taken, such that the different variance of measurements at each time point is incorporated into the objective function:

$$\text{objective}_{WLS} = \sum_{i=1}^n \frac{1}{\sigma_{t_i}} (y_i - g_j(x, t_i))^2 \quad (3.4)$$

²One of the cases where it is not possible is when the approximate problem is not locally convex near the current iterate.

³Also called a Newton step.

Here, $g_j(x, t_i)$ is the ode45-solution of our differential equation(s) with parameters x at time t_i . If the variance is small, the weight $\frac{1}{\sigma}$ is greater than for distantly scattered measurements, such that the influence of what is assumed to have been less prone to noise is valued more. The initial conditions NSC_0 or $(\text{aNSC}, \text{qNSC})_0$ for the both systems have also been parameters to be estimated by `fmincon`. In the case of the AaQNSC model the total number of NSCs at day 0, NSC_0 , served as an input to the objective function. The steady state which is derived in the fraction chapter 4 was used to compute the separate amounts of active and quiescent cell numbers' initial value aNSC_0 and qNSC_0 from NSC_0 . This results in the initial ratio of $\frac{\text{aNSC}}{\text{NSC}}$ being dependent on the parameters (r, b) , $r(0)$ or $b(0)$.

3.3 Model comparison

In order to assess which model represents our data best, while also considering the trade-off between goodness of fit and complexity of the model, the Akaike Information Criterion (Akaike, 1998) was applied [2]. In the following, I will address the AIC and its corrected version, the AICc, which is an adaptation for smaller sample sizes. For each model g_j the AIC is defined as

$$\text{AIC} = n \ln \left(\frac{\sum \hat{\varepsilon}_i}{n} \right) + 2k \quad (3.5)$$

where n is the total number of measured datapoints, k is the number of parameters and $\hat{\varepsilon}_i$ are the weighted residuals⁴ of those datapoints, i.e.

$$\hat{\varepsilon}_i = \frac{1}{\sigma_i} (g_j(\hat{x}, t_i) - y_i),$$

where t_i is the time at which the datapoint y_i has been measured [1, 3]. The AIC is constructed such that Overfitting⁵ is avoided, as the AIC value increases for a higher number of parameters, thus favouring models with smaller number of parameters [4]. The corrected version for small sample sizes is

$$\text{AICc} = \text{AIC} + \frac{2k^2 + 2k}{n - k - 1} \quad (3.6)$$

where, as before, k is the number of parameters the model g_j depends on [21]. The additional term in (3.6) modifies the rating such that it becomes infinite when the number of parameters k gets close to the number of data points n minus one. The actual AIC or AICc values do not matter absolutely, they merely give a relative rating of different models/model variations,

⁴The hat emphasizes that those are the residuals of optimized parameters \hat{x} in contrast to the residuals in the objective function which is needed to find those 'optimal' parameters.

⁵When the fit adjusts to the noise of the measurements, due to a too high number of parameters in the model.

and we consider the value only in relation to the smallest AIC: $\Delta_j = \text{AIC}_j - \text{AIC}_{\min}$.

3.4 Experimental data

The data used in this thesis have been provided by the group of Prof. Dr. Martin-Villalba and described by Kalamakis in [10]. Three different experimental setups were used. To count the number of NSCs, aNSCs and qNSCs, the SVZ of mice was dissected and the cells in a single cell suspension were counted via fluorescence-activated cell sorting (FACS). Antibodies of various types were used to stain the sample. Due to the significant cell loss associated with this method, the fractions of active vs. quiescent cells were also determined using immunohistostaining. This procedure was repeated three times for mice of various ages. In short, in this work, two time-series datasets have been used:

- the total number of NSCs at timepoints 60 days (6 mice), 210 days (3 mice), and 660 days (3 mice)
- the fraction of active cells among label-retaining cells at 60 days (3 mice), 210 days (2 mice), and 660 days (3 mice), which is an approximation of the fraction $\frac{\text{aNSC}}{\text{NSC}}$

4 The fractions

In chapter 2 we introduced the AaQNSC model of ordinary differential equations to model the number of quiescent and active NSCs in the ventricular/subventricular zone:

$$\begin{pmatrix} \text{qNSC} \\ \text{aNSC} \end{pmatrix}' = \begin{pmatrix} -r & 2bp \\ r & -p \end{pmatrix} \begin{pmatrix} \text{qNSC} \\ \text{aNSC} \end{pmatrix} \quad (4.1)$$

Studying this system for **constant** parameters one can also inspect the derived ODEs of the fractions

$$\frac{\text{aNSC}}{\text{aNSC}+\text{qNSC}}(t) \quad \text{and} \quad \frac{\text{qNSC}}{\text{aNSC}+\text{qNSC}}(t). \quad (4.2)$$

For simplicity, in the following we denote $A := \text{aNSC}$ and $Q := \text{qNSC}$. By using the product rule of differentiation, by inserting the equation (4.1) and by the identity $\frac{Q}{Q+A} = 1 - \frac{A}{Q+A}$ we get

$$\begin{aligned} \left(\frac{A}{Q+A} \right)' &= \frac{A'}{Q+A} - \frac{A}{(Q+A)^2}(Q' + A') \\ &= \frac{rQ - pA}{Q+A} - \frac{A}{(Q+A)^2}(2b-1)pA \\ &= r\frac{Q}{Q+A} - p\frac{A}{Q+A} - (2b-1)p\left(\frac{A}{Q+A}\right)^2 \\ &= r\left(1 - \frac{A}{Q+A}\right) - p\frac{A}{Q+A} - (2b-1)p\left(\frac{A}{Q+A}\right)^2. \end{aligned} \quad (4.3)$$

Denoting the fraction $\frac{A}{Q+A}$ as F_A we get a single nonlinear ODE

$$F_A' = r - (r+p)F_A + (1-2b)pF_A^2. \quad (4.4)$$

Analogously, for $F_Q := \frac{Q}{Q+A}$ we get

$$\begin{aligned} F_Q' &= \left(\frac{Q}{Q+A} \right)' = \frac{Q'}{Q+A} - \frac{Q}{(Q+A)^2}(A' + Q') \\ &= \frac{-rQ + 2bpA}{Q+A} - \frac{Q}{(Q+A)^2}(2b-1)pA \\ &= -r\frac{Q}{Q+A} + 2bp\frac{A}{Q+A} - \frac{Q}{Q+A}(2b-1)p\frac{A}{A+Q} \\ &= -rF_Q + 2bp(1-F_Q) - F_Q(2b-1)p(1-F_Q) \\ &= -rF_Q + 2bp - 2bpF_Q - (2b-1)pF_Q + (2b-1)pF_Q^2 \\ &= 2bp - (r-p+4bp)F_Q + (2b-1)pF_Q^2. \end{aligned} \quad (4.5)$$

4.1 The equilibrium points of $\frac{A}{Q+A}$

For this chapter, we define

$$f : \mathbb{R} \rightarrow \mathbb{R} \text{ with } f(F_A) := r - (r+p)F_A + (1-2b)pF_A^2 \quad (4.6)$$

for r, b in $(0, 1)$.

This corresponds to our nonlinear, autonomous, ordinary differential equation (4.4). In the following we will distinguish three cases of b in relation to $\frac{1}{2}$, as they have rather different implications for the following examination. For the sake of completeness all three cases will be mathematically examined, although all of the observed data suggests $b < \frac{1}{2}$.

case 1: $b < \frac{1}{2}$ Equation (4.6) has two equilibrium points, i.e. points in which the solution to the differential equation is constant, namely

$$F_{A_{1,2}}^* = \frac{(r+p) \pm \sqrt{(r+p)^2 - 4(1-2b)pr}}{2(1-2b)p} \quad (4.7)$$

To obtain the local behaviour of the solutions in the phase space near our equilibria we take a look at the linearization (4.8) of our problem (4.4) at those equilibria and confirm that no eigenvalue λ_i of the linearization has a real part equal to 0 (4.9)⁶.

$$(Df)(F_{A_i}^*) = \pm \sqrt{(r+p)^2 - 4(1-2b)pr} =: \lambda_i \quad (i = 1, 2). \quad (4.8)$$

$$\begin{aligned} (r+p)^2 - 4(1-2b)pr &> 0 \\ \Leftrightarrow (r+p)^2 + 8bpr - 4pr &> 0 \\ \Leftrightarrow r^2 + p^2 + 2pr + 8bpr - 4pr &> 0 \\ \Leftrightarrow r^2 + p^2 - 2pr + 8bpr &> 0 \\ \Leftrightarrow (r-p)^2 + 8bpr &> 0 \end{aligned} \quad (4.9)$$

which is true as $r, b \in (0, 1)$.

As this is the case, the Hartman–Grobman theorem can be applied, stating that locally the non-linear system behaves like the linearized system for the two hyperbolic⁷ equilibria [5]. The stability of those equilibria of the linearized problems corresponds to the stability of the equilibria of (4.6) in the following way: Due to the principle of linear stability, $F_{A_i}^*$ ($i = 1, 2$)

⁶If the squared term of the linearization is strictly positive, the eigenvalues are strictly positive or negative.

⁷A hyperbolic equilibrium is one for which the eigenvalues are non-zero.

is an asymptotically stable equilibrium if

$$Re(\lambda_{1,2}) = Re(\pm\sqrt{(r+p)^2 - 4(1-2b)pr}) < 0 \quad (4.10)$$

and an unstable equilibrium if the opposite holds. Now, considering the second equilibrium point $F_{A_2}^*$ we get that it is a stable equilibrium of (4.8, $i = 2$), due to (4.9), while $F_{A_1}^*$ is an unstable equilibrium of (4.6).

As F_A is a fraction, it is assumed to be in $[0,1]$, so it is interesting to check where our equilibria are situated in relation to 0, 1 and also to each other. For $b < \frac{1}{2}$ the denominator of our equilibria is positive, such that $F_{A_1}^* > F_{A_2}^*$. It is also true that $F_{A_2}^* > 0$ as

$$\begin{aligned} F_{A_2}^* &> 0 \\ \Leftrightarrow (r+p) - \sqrt{(r+p)^2 - 4(1-2b)pr} &> 0 \\ \Leftrightarrow (r+p) &> \sqrt{(r+p)^2 - 4(1-2b)pr} \\ \Leftrightarrow (r+p)^2 &> (r+p)^2 - 4(1-2b)pr \\ \Leftrightarrow 4(1-2b)pr &> 0 \end{aligned} \quad (4.11)$$

Figure 2 shows $F_{A_1}^*$ and $F_{A_2}^*$ plotted for different values of (r, b) in $(0, 1) \times (0, \frac{1}{2})$. Computation

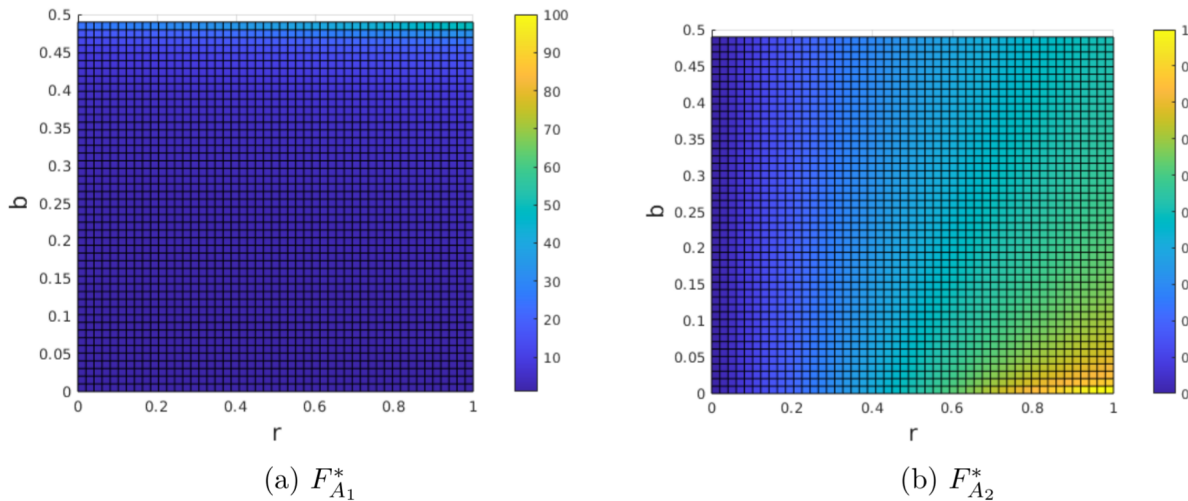


Figure 2: $F_{A_1}^*$ and $F_{A_2}^*$ for $b < \frac{1}{2}$

shows that the minimal $F_{A_1}^*$ is 1 while the maximal $F_{A_1}^*$ is around 100. The minimal $F_{A_2}^*$ is 0 (which only occurs for $r = 0$) and the maximal $F_{A_2}^*$ is 1. $F_{A_1}^*$ is not biologically relevant, since $F_A = \frac{A}{Q+A}$ should lie in $[0, 1]$. In figure 3 you see the phase diagram of our solution to (4.3).

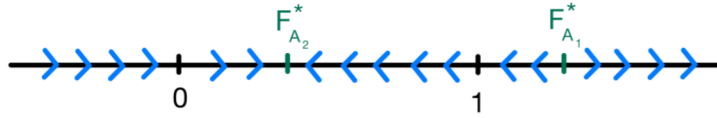


Figure 3: Sketch of the phase diagram for $b < \frac{1}{2}$

case 2: $b > \frac{1}{2}$ Similarly to the case $b < \frac{1}{2}$ the equation 4.6 has the equilibrium points

$$F_{A_{1,2}}^* = \frac{(r+p) \pm \sqrt{(r+p)^2 - 4(1-2b)pr}}{2(1-2b)p} \tag{4.12}$$

and those equilibrium points have the same stability properties as those in case $b < \frac{1}{2}$, i.e. $F_{A_2}^*$ is asymptotically stable and $F_{A_1}^*$ is unstable. Figure 4 shows $F_{A_1}^*$ and $F_{A_2}^*$ plotted for different values of (r, b) in $(0, 1) \times (\frac{1}{2}, 1)$: Computation shows that the minimal $F_{A_1}^*$ is approximately

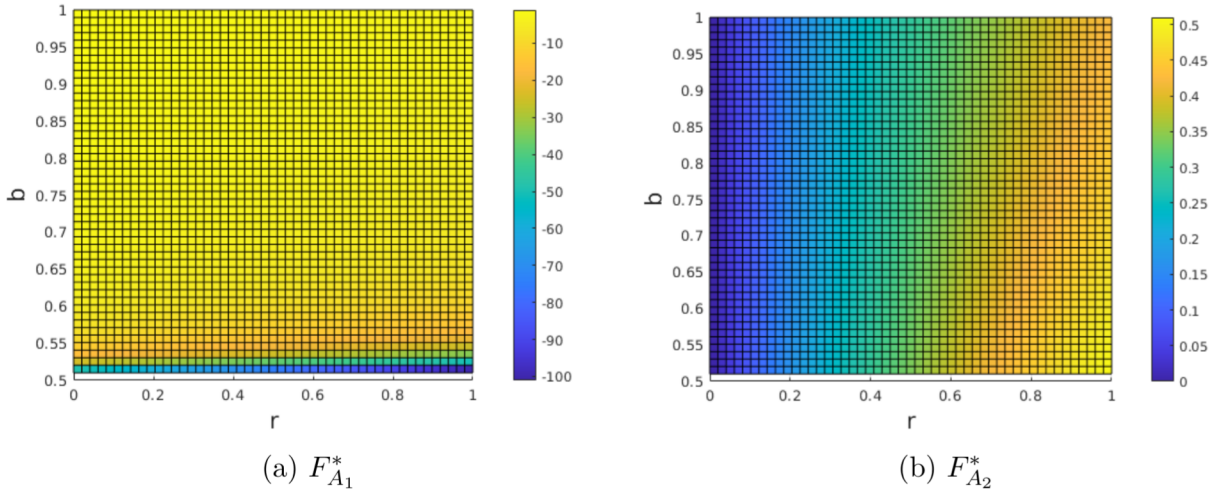


Figure 4: $F_{A_1}^*$ and $F_{A_2}^*$ for $b > \frac{1}{2}$

-100 while the maximal $F_{A_1}^*$ is below -1. The minimal $F_{A_2}^*$ is 0 and the maximal $F_{A_2}^*$ is approximately $\frac{1}{2}$. As before, the unstable equilibrium $F_{A_1}^* < 0$ is not biologically relevant.

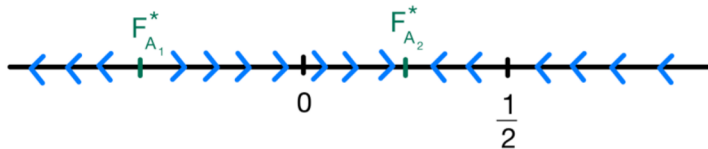


Figure 5: Sketch of the phase diagram for $b > \frac{1}{2}$

case 3: $b = \frac{1}{2}$ This assumption changes our model significantly as our system of equations (4.1) becomes

$$\begin{pmatrix} \text{qNSC} \\ \text{aNSC} \end{pmatrix}' = \begin{pmatrix} -r & p \\ r & -p \end{pmatrix} \begin{pmatrix} \text{qNSC} \\ \text{aNSC} \end{pmatrix} \quad (4.13)$$

which statistically looks as if for each quiescent cell becoming active we 'get' one quiescent cell such that the sum of active and quiescent cells stays constant:

$$(\text{qNSC} + \text{aNSC})' = -r\text{qNSC} + p\text{aNSC} + r\text{qNSC} - p\text{aNSC} = 0 \quad (4.14)$$

Our equation (4.6) becomes

$$\left(\frac{A}{Q+A}\right)' = r - (r+p)\left(\frac{A}{Q+A}\right) \quad (4.15)$$

which is solved by

$$\left(\frac{A}{Q+A}\right)(t) = F_A(t) = e^{-(r+p)t} \left(F_A(0) - \frac{r}{r+p}\right) + \frac{r}{r+p}, \quad t > 0, \quad (4.16)$$

(4.15) has the equilibrium $F_A^* = \frac{r}{r+p}$ which due to $\left(\frac{A}{Q+A}\right)' \Big|_{F_A^*} = -(r+p) < 0$ is a sink, meaning all solutions in the phase space converge to $\frac{r}{r+p}$. $b = \frac{1}{2}$ is a bifurcation.

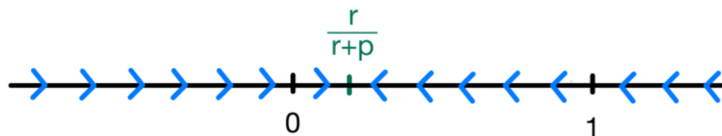


Figure 6: Sketch of the phase diagram for $b = \frac{1}{2}$

4.2 The convergence of $\frac{A}{Q+A}$

In the previous section we analysed the phase space of equation (4.6) in the constant scenario of the AaQNSc model and showed that for $(r, b) \in (0, 1) \times (0, \frac{1}{2})$ the solutions converge to a steady state $F_{A_2}^*$. In order to check how fast this happens we generated random values for $(r, b, qNSC_0, aNSC_0) \in (0, 1) \times (0, \frac{1}{2}) \times (0, 1000) \times (0, 1000)$ via uniform sample and plotted the solutions to equation (4.3) (Figure 7). It is easy to see that the displayed functions reach their equilibrium point after some days, so $\frac{\text{aNSC}}{\text{NSC}} = F_{A_2}^*$ is a close approximation in the constant scenario.

$$\begin{pmatrix} qNSC \\ aNSC \end{pmatrix}' = \begin{pmatrix} -r & 2bp \\ r & -p \end{pmatrix} \begin{pmatrix} qNSC \\ aNSC \end{pmatrix} \quad (4.17)$$

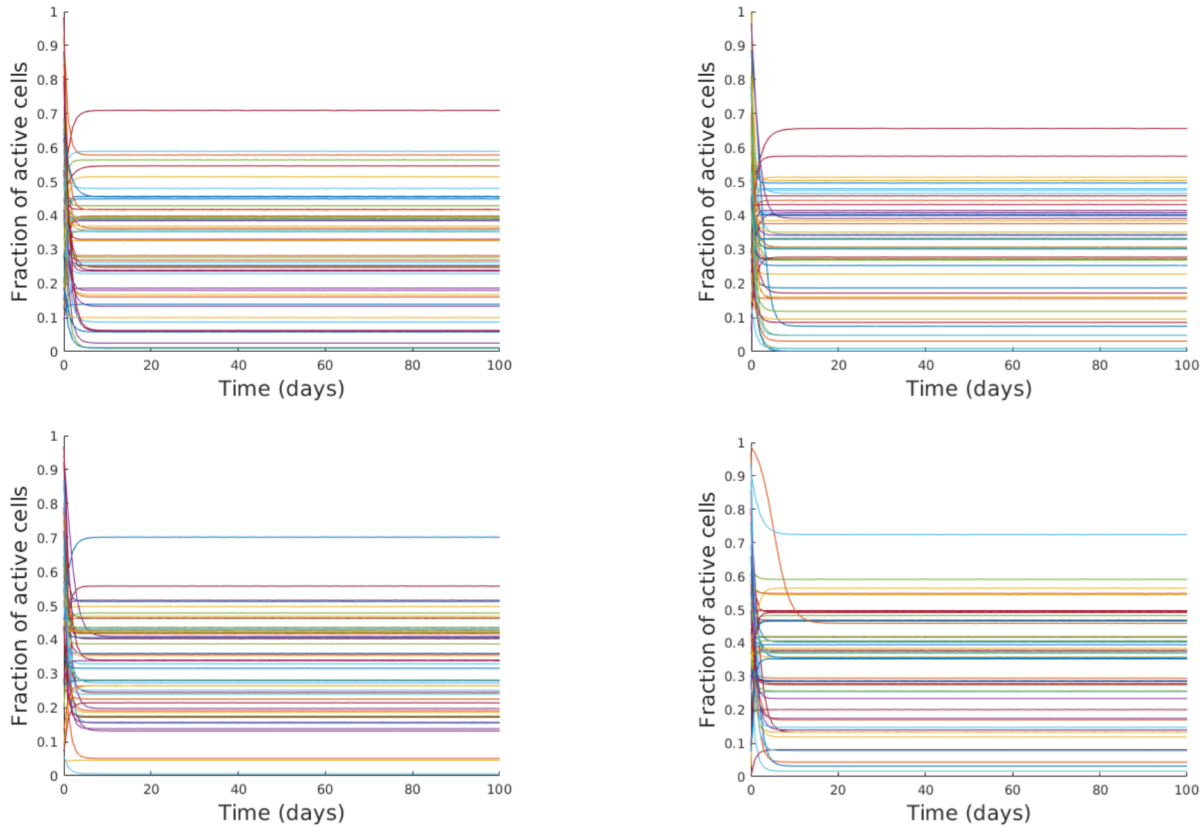


Figure 7: $\frac{A}{Q+A}$ over time for different, randomly chosen parameters ($r, b, qNSC_0, aNSC_0$)

4.3 Application of the fraction results

In previous chapters we introduced two models for cell population development of neural stem cells.

$$\frac{d}{dt} \begin{pmatrix} \text{qNSC} \\ \text{aNSC} \end{pmatrix} (t) = \begin{pmatrix} -r & 2bp \\ r & -p \end{pmatrix} \begin{pmatrix} \text{qNSC} \\ \text{aNSC} \end{pmatrix} (t) \quad \left| \quad \begin{aligned} \frac{d}{dt} \text{NSC}(t) &= (2a - 1)p \text{NSC}(t) \\ a &\in \left(0, \frac{1}{2}\right) \end{aligned} \right.$$

$$b \in \left(0, \frac{1}{2}\right), r \in (0, 1)$$

We derived a stable equilibrium for constant parameters to which the fraction converges for any of our parameters $r \in (0, 1), b \in (0, \frac{1}{2})$. As shown in figure 7 the fraction converges really fast to the equilibrium point, so we use the approximation

$$\frac{A}{Q+A} = F_{A_2}^* \Leftrightarrow Q+A = \frac{A}{F_{A_2}^*} \quad (4.18)$$

which can be inserted into our one equation model in the following way:

$$\begin{aligned} \frac{d}{dt}S &= (2a - 1)pS = (2a - 1)p(Q + A) = (2a - 1)p\frac{A}{F_{A_2}^*} \\ &\parallel \\ \frac{d}{dt}(Q + A) &= (2b - 1)pA = (2b - 1)pF_{A_2}^*(A + Q) \end{aligned} \quad (4.19)$$

so

$$\begin{aligned} (2a - 1)p\frac{A}{F_{A_2}^*} &= (2b - 1)pF_{A_2}^*(A + Q) \\ \Leftrightarrow (2a - 1) &= (2b - 1)F_{A_2}^* \\ \Leftrightarrow a &= \frac{(2b - 1)F_{A_2}^* + 1}{2} \end{aligned} \quad (4.20)$$

and a and (r, b) are related in the following way

$$\begin{aligned} \Leftrightarrow a &= \frac{1}{2} \left[(2b - 1) \frac{(r + p) - \sqrt{(r + p)^2 - 4(1 - 2b)pr}}{2(1 - 2b)p} + 1 \right] \\ &= \frac{1}{2} + \frac{(r + p)}{-4p} + \frac{\sqrt{(r + p)^2 - 4(1 - 2b)pr}}{4p} \\ &= \frac{1}{4} - \frac{r}{4p} + \frac{\sqrt{(r + p)^2 - 4(1 - 2b)pr}}{4p} \end{aligned} \quad (4.21)$$

We define

$$a : (0, 1) \times \left(0, \frac{1}{2}\right) \rightarrow (0, 1) \text{ with } a(r, b) := \frac{1}{4} - \frac{r}{4p} + \frac{\sqrt{(r + p)^2 - 4(1 - 2b)pr}}{4p} \quad (4.22)$$

and consider the problem

$$\frac{d}{dt} \text{NSC}(t) = (2a(r, b) - 1)p \text{NSC}(t). \quad (4.23)$$

Furthermore, we include the time-dependency of r and/or b to do parameter estimations with the one equation model with varying a : $a(r, b), a(r, b(t)), a(r(t), b), a(r(t), b(t))$. This is certainly only an approximate model, but the goal is to see how much of the original AaQNSC dynamics can be captured with such a simplified model. ODE (4.23) has a unique solution for a given initial value NSC_0 , also in any aging scenario. This kind of merged model will be referred to as the **MTNSC** model.

5 Results of the parameter estimations

5.1 Comparing AaQNSC and TNSC model variations

To clarify that the parameter estimation implementation works correctly the results have been compared to those of Kalamakis et al. (2019), which confirmed that the code is working properly, as the AaQNSC parameters are approximately the same.

Mechanism	Parameter	Kalamakis et al.	AaQNSC
No aging	r	0,278	0,22
	b	0,489	0,493
Increasing self-renewal	r	0,28	0,28
	b_{min}	0,0049	0,46
	β_b	0,0276	$6,8 \cdot 10^{-3}$
Increasing quiescence	r_{max}	0,453	0,458
	β_r	$9,5 \cdot 10^{-4}$	$9,7 \cdot 10^{-4}$
	b	0,494	0,492
Increasing quiescence and self-renewal	r_{max}	0,445	0,444
	β_r	$9,2 \cdot 10^{-4}$	$9,1 \cdot 10^{-4}$
	b_{min}	0,489	0,473
	β_b	0,0022	$5,7 \cdot 10^{-3}$

Table 1: Comparison of parameter estimation results

The plots of total number of NSCs and fraction of active cells over total number of NSCs are shown in the following figure:

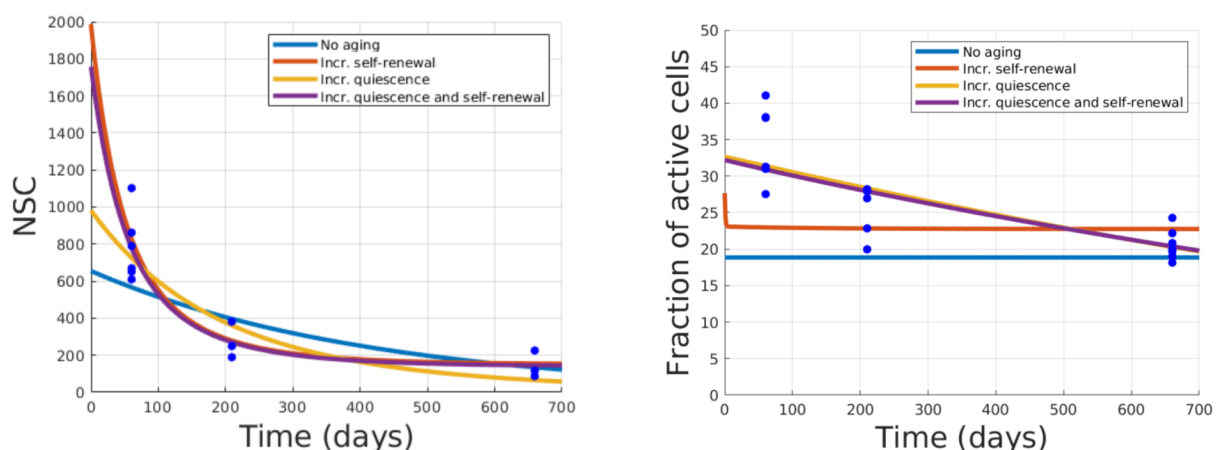


Figure 8: AaQNSC model fits

The graph of the fraction in the 'Increasing self-renewal' scenario shows a rapid drop at the beginning, which can be explained with the initial fraction $\frac{a_{NSC}}{NSC}$ being estimated with the

steady state from chapter 4, which is an approximation derived from the 'No aging' scenario⁸. As already observed by Kalamakis et al. (2019), only the scenarios 'Increasing quiescence' and 'Increasing quiescence and self-renewal' captured the time-dependent decrease of the fraction adequately [10].

Model	Mechanism	Parameters	ΔAICc
AaQNSC	Increasing quiescence and self-renewal (b)	$r_{max} = 0,444$ $\beta_r = 9,1 \cdot 10^{-4}$ $b_{min} = 0,473$ $\beta_b = 5,7 \cdot 10^{-3}$ $NSC_0 = 1757$	0
	Increasing quiescence	$r_{max} = 0,458$ $\beta_r = 9.7 \cdot 10^{-4}$ $b = 0,492$ $NSC_0 = 981$	3
	Increasing self-renewal (b)	$r = 0,28$ $b_{min} = 0,46$ $\beta_b = 6.8 \cdot 10^{-3}$ $NSC_0 = 1869$	19.33
	No aging	$r = 0,22$ $b = 0,493$ $NSC_0 = 655$	33.6

Table 2: Model Comparison of AaQNSC model variations

The parameter estimation in the case of the TNSC model resulted in the curves shown in figure 9. Introducing an increasing $a(t)$ self-renewal ratio in the TNSC model improved the TNSC model resulting in an adequate fit of stem cells. Per definition, the TNSC model alone is not capable of depicting the ratio $\frac{aNSC}{NSC}$.

⁸For which it is also merely an approximation, but certainly more accurate as the same mechanism is the foundation of the approximation.

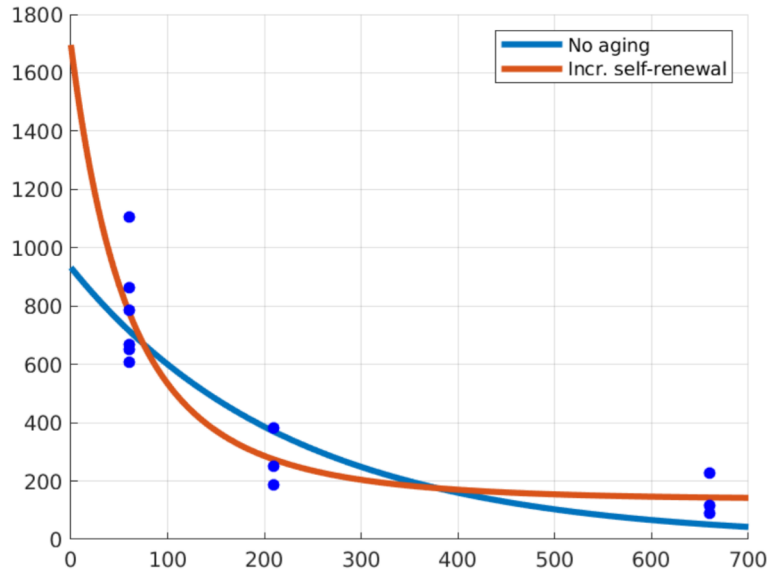


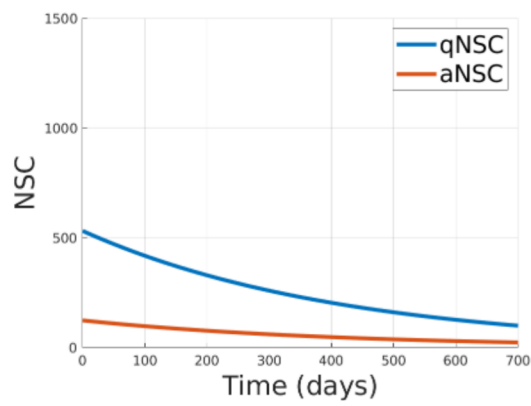
Figure 9: TNSC model variations

Computing the AICc's (see figure 3) for the TNSC model variations suggests the time-dependent TNSC model variation as a better trade-off between simplicity and minimal error. There is a lot less information covered in the TNSC model as it provides no output about the amount of cells proliferating.

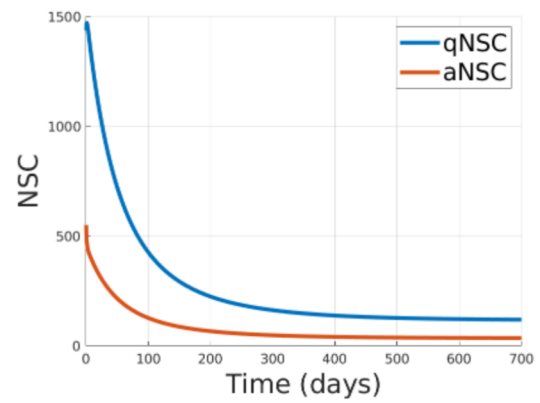
Model	Mechanism	Parameters	ΔAICc
TNSC	Increasing self-renewal (a)	$a_{min} = 0,492$ $\beta_a = 6.7 \cdot 10^{-3}$ $NSC_0 = 1695$	0
	No aging	$a = 0,498$ $NSC_0 = 932$	4.2

Table 3: Model Comparison of TNSC model variations

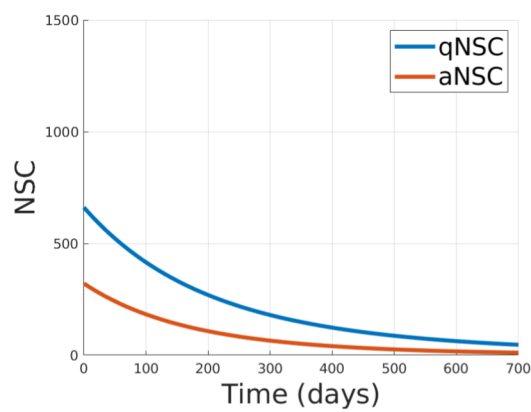
To visualize the additional information captured in the AaQNSC model, figure 10 shows the amounts of active and quiescent NSCs we get as a result for fitted parameters.



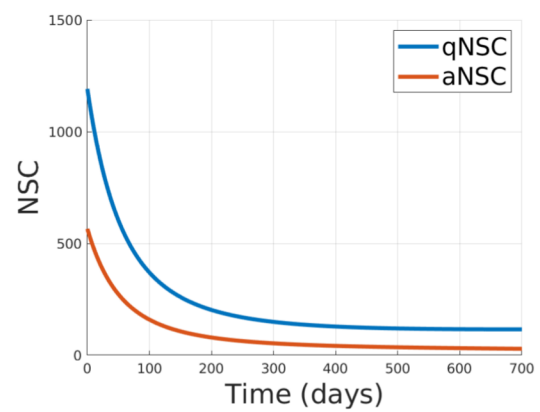
(a) No aging



(b) Increasing self-renewal



(c) Increasing quiescence



(d) Increasing quiescence and self-renewal

Figure 10: AaQNSC fits of active and quiescent NSCs

5.2 Merged TNSC model

Another aim of this thesis was to study the relation between the TNSC and AaQNSC model (in particular the relation of the parameters) and for that purpose a Merged TNSC (MTNSC) model has been introduced:

$$\frac{d}{dt} \text{NSC}(t) = (2a(r, b) - 1)p \text{NSC}(t)$$

$$\text{where } a(r, b) := \frac{1}{4} - \frac{r}{4p} + \frac{\sqrt{(r+p)^2 - 4(1-2b)pr}}{4p} \quad (5.1)$$

$$\text{for } r, b \in (0, 1) \times (0, \frac{1}{2})$$

First, to ensure that the MTNSC model with its parameters represents the structure of the AaQNSC model, it is plotted for the optimal AaQNSC parameters. Figure 11 shows that indeed the MTNSC model recapitulates the behaviour of the AaQNSC, as expected.

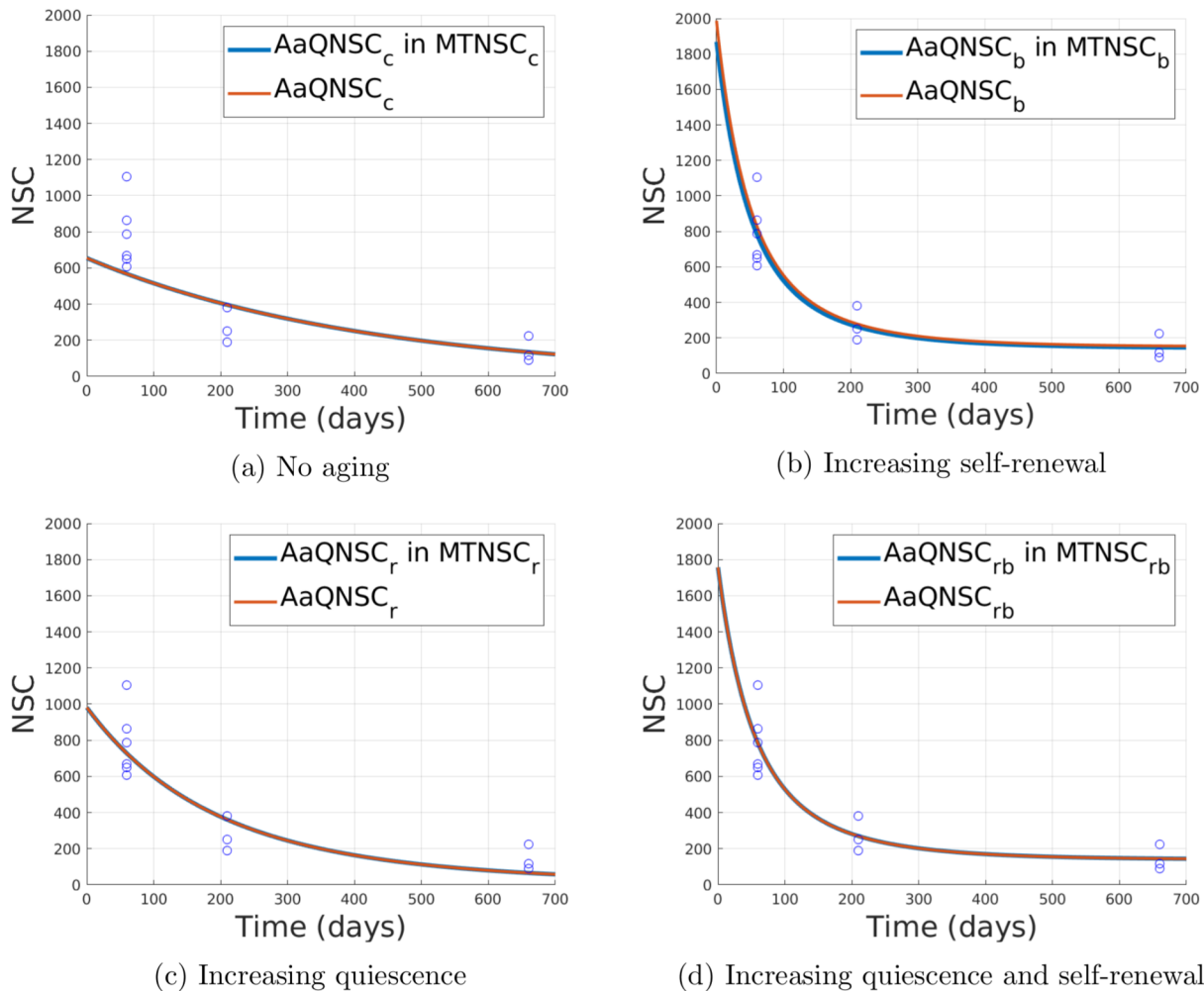


Figure 11: AaQNSC fits and MTNSC model with AaQNSC parameters. The subscript in each legend suggests which parameter is time-dependent.

By estimating the parameters, we observe that the MTNSC model on its own is capable of matching the NSC data adequately for all time-dependent mechanisms, but not for the constant scenario. The results of the MTNSC parameter estimation are shown in figure 12.

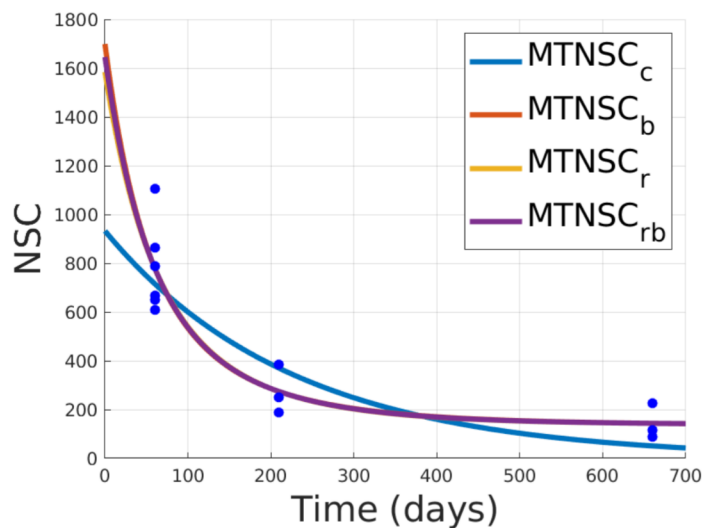


Figure 12: MTNSC fits

In terms of AICc rating, the 'Increasing quiescence' and 'Increasing self-renewal' MTNSC model variations surpass the other scenarios. This happens because the fits of all 3 model variations with time-dependent parameters are quite similar, such that the additional parameter is taken into account more severely.

Model	Mechanism	Parameters	ΔAIC_c
MTNSC	Increasing quiescence	$r_{max} = 0,374$ $\beta_r = 6,7 \cdot 10^{-3}$ $b = 0,487$ $NSC_0 = 1611$	0
	Increasing self-renewal	$r = 0,487$ $b_{min} = 0,488$ $beta_b = 6,2 \cdot 10^{-3}$ $NSC_0 = 1697$	0
	No aging	$r = 0,966$ $b = 0,488$ $NSC_0 = 932$	3,2
	Increasing quiescence and self-renewal (b)	$r_{max} = 0,414$ $beta_r = 3.5 \cdot 10^{-3}$ $b_{min} = 0,487$ $beta_b = 3.2 \cdot 10^{-3}$ $NSC_0 = 1658$	6,3

Table 4: Model Comparison of MTNSC model variations

To check how the parameters' purpose changes in the MTNSC model, the optimal MTNSC parameters were input into the AaQNSC model, such that the total number of NSCs **and** the fractions $\frac{a_{NSC}}{NSC}$ could be observed (Figure 13).

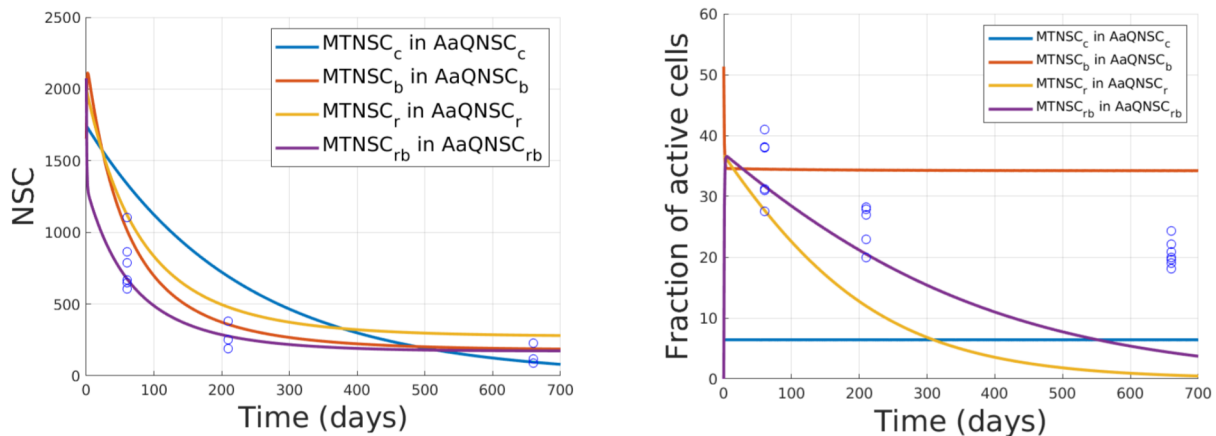


Figure 13: AaQNSC model with MTNSC parameters

While one can observe that the total number of NSCs in the MTNSC model is fitted nicely (see figure 12), the plots worsen a lot when those same parameters are used in the AaQNSC model, although the same NSC data is used to produce the fits. This however is easily understandable when one looks at how $a(r, b)$ looks for different parameters r and b

(Figure 14).

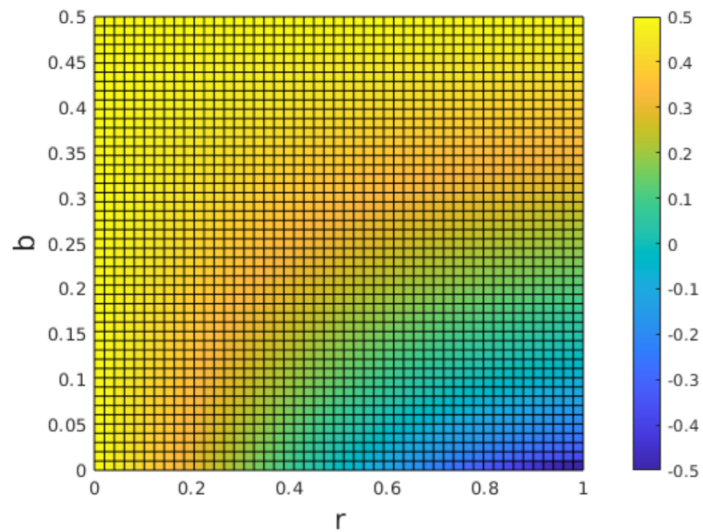


Figure 14: $a(r,b)$

Many completely different combinations of the parameters r and b lead to the same macroscopic a , such that the information of those separate rates gets lost in the process of estimation. In other words, parameter a is non-identifiable with respect to r and b [15]. For the fractions, the MTNSC model does not capture the behavior at all, which is understandable as the data used to fit the model only consists of total numbers of NSC observations, and does not take into account the fractions of $\frac{a_{\text{NSC}}}{\text{NSC}}$.

6 Final remarks

Adult neurogenesis in the V-SVZ⁹ is an important process supplying the olfactory bulb with new neurons throughout life and serving as a backup in the event of damage or trauma. It is not fully understood how the supply of adult neural stem cells keeps slowly declining, neither saturating nor draining, while undergoing ageing effects. Models of neurogenesis via ordinary differential equations include ageing-related effects by introducing time-dependent parameters, observing which parameters explain the systems dynamics and lead to minimal deviation from the data. Previous research by Kalamakis et al.(2019) suggested a decreasing activation rate $r(t)$ with age ('Increasing quiescence') to be the best explanation and trade-off between simplicity and error. Parameter estimation computes an initial amount of about 1000 NSCs at birth and shows a small decline in stem cell numbers compared to a scenario with 'increasing self-renewal' $b(t)$, where initial NSCs are estimated to be around 2000. The combination of both mechanisms is able to improve the fit with more reasonable estimated initial conditions.

In this thesis, a one-equation neurogenesis model governed by a macroscopic fraction of self-renewal (a) as in the hematopoiesis model by Stiehl et al. (2012, 2014) has been studied in its ability to explain the experimental data. Introducing a time-dependent self-renewal ratio $a(t)$ improved the fit to match the experimental observations. While it reflects the data, the model (by definition) does not inherit the ability to describe the fraction of active cells. A steady-state of the fraction of active NSCs over NSCs has been derived, and served to build a merged model. The newly built model relates the self-renewal (b or b_{min}, β_b) and activation (r or r_{max}, β_r) parameters of the Kalamakis et al. (2019) model with the macroscopic self-renewal (a) parameter as in the model by Stiehl et al. (2012, 2014) and matches the experimental data. It is not inherently unable to give information about the fraction of active cells, but does not reflect the fraction data, as it is simply not fitted to it, due to the model description via one single differential equation. Furthermore, the relation of the parameters illustrates the loss of information moving from a two-dimensional into a one-dimensional space. For any model, observing the number of NSCs at day 0 experimentally can lead to more accurate fits and fraction data at day 0 is valuable for fitting the AaQNSC model, possibly scaling down the error that might occur from estimating the initial fraction with the steady-state of the 'No aging' scenario. Also, additional data especially for more (early) time points would be useful in determining how quickly cell counts decrease in the beginning. Data from later time points would reveal if the cell counts achieve any saturation or continue to decline until death.

⁹As neurogenesis in the hippocampus shows similar behaviour the models evaluated in this study can lead to better insights in both brain regions, the ventricular-subventricular zone and the hippocampus.

References

- [1] Hirotugu Akaike. “A new look at the statistical model identification”. In: *IEEE Transactions on Automatic Control* 19 (1974), pp. 716–723.
- [2] Hirotugu Akaike. *Information Theory and an Extension of the Maximum Likelihood Principle*. 1998. DOI: https://doi.org/10.1007/978-1-4612-1694-0_15.
- [3] Hirotugu Akaike. “On the Likelihood of a Time Series Model”. In: *The Statistician* 27 (1978), pp. 289–307.
- [4] Kenneth P. Burnham and David R. Anderson. “Multimodel Inference: Understanding AIC and BIC in Model Selection”. In: *Sociological Methods & Research* 33.2 (2004), pp. 261–304. DOI: 10.1177/0049124104268644. URL: <https://doi.org/10.1177/0049124104268644>.
- [5] Wikipedia contributors. *Hartman–Grobman theorem — Wikipedia, The Free Encyclopedia*. [Online; accessed 1-March-2022]. 2022. URL: https://en.wikipedia.org/w/index.php?title=Hartman%E2%80%93Grobman_theorem&oldid=1068276148.
- [6] Fiona Doetsch et al. “Subventricular Zone Astrocytes Are Neural Stem Cells in the Adult Mammalian Brain”. In: *Cell* 97.6 (1999), pp. 703–716. ISSN: 0092-8674. DOI: [https://doi.org/10.1016/S0092-8674\(00\)80783-7](https://doi.org/10.1016/S0092-8674(00)80783-7). URL: <https://www.sciencedirect.com/science/article/pii/S0092867400807837>.
- [7] J.R. Dormand and P.J. Prince. “A family of embedded Runge-Kutta formulae”. In: *Journal of Computational and Applied Mathematics* 6.1 (1980), pp. 19–26. ISSN: 0377-0427. DOI: [https://doi.org/10.1016/0771-050X\(80\)90013-3](https://doi.org/10.1016/0771-050X(80)90013-3). URL: <https://www.sciencedirect.com/science/article/pii/0771050X80900133>.
- [8] Xiang Gao, Grigori Enikolopov, and Jinhui Chen. “Moderate traumatic brain injury promotes proliferation of quiescent neural progenitors in the adult hippocampus”. In: *Experimental Neurology* 219.2 (2009), pp. 516–523. ISSN: 0014-4886. DOI: <https://doi.org/10.1016/j.expneurol.2009.07.007>. URL: <https://www.sciencedirect.com/science/article/pii/S0014488609002702>.
- [9] Brian Ingalls. *Mathematical modeling in systems biology: An introduction*. 2013.
- [10] Georgios Kalamakis et al. “Quiescence Modulates Stem Cell Maintenance and Regenerative Capacity in the Aging Brain”. In: *Cell* 176.6 (2019), 1407–1419.e14. ISSN: 0092-8674. DOI: <https://doi.org/10.1016/j.cell.2019.01.040>. URL: <https://www.sciencedirect.com/science/article/pii/S0092867419301035>.

- [11] Daniel A. Lim and Arturo Alvarez-Buylla. “The Adult Ventricular–Subventricular Zone (V-SVZ) and Olfactory Bulb (OB) Neurogenesis”. In: *Cold Spring Harbor Perspectives in Biology* 8.5 (2016). DOI: 10.1101/cshperspect.a018820. eprint: <http://cshperspectives.cshlp.org/content/8/5/a018820.full.pdf+html>. URL: <http://cshperspectives.cshlp.org/content/8/5/a018820.abstract>.
- [12] E. Lindelöf. “Sur l’application de la méthode des approximations successives aux équations différentielles ordinaires du premier ordre”. In: *Comptes rendus hebdomadaires des séances de l’Académie des sciences* 118 (1894), pp. 454–457.
- [13] *MATLAB version 9.10.0.1649659 (R2021a) Update 1*. Natick, Massachusetts: The MathWorks Inc., 2021.
- [14] Guo-li Ming and Hongjun Song. “Adult Neurogenesis in the Mammalian Brain: Significant Answers and Significant Questions”. In: *Neuron* 70.4 (2011), pp. 687–702. ISSN: 0896-6273. DOI: <https://doi.org/10.1016/j.neuron.2011.05.001>. URL: <https://www.sciencedirect.com/science/article/pii/S0896627311003485>.
- [15] R. Muñoz-Tamayo et al. “Review: To be or not to be an identifiable model. Is this a relevant question in animal science modelling?” In: *Animal* 12.4 (2018), pp. 701–712. ISSN: 1751-7311. DOI: <https://doi.org/10.1017/S1751731117002774>. URL: <https://www.sciencedirect.com/science/article/pii/S1751731117002774>.
- [16] Kirsten Obernier et al. “Adult Neurogenesis Is Sustained by Symmetric Self-Renewal and Differentiation”. In: *Cell Stem Cell* 22.2 (2018), 221–234.e8. ISSN: 1934-5909. DOI: <https://doi.org/10.1016/j.stem.2018.01.003>. URL: <https://www.sciencedirect.com/science/article/pii/S1934590918300031>.
- [17] Giovanna Ponti, Kirsten Obernier, and Arturo Alvarez-Buylla. “Lineage progression from stem cells to new neurons in the adult brain ventricular-subventricular zone”. In: *Cell cycle (Georgetown, Tex.)* 12 (May 2013). DOI: 10.4161/cc.24984.
- [18] Matlab R2021b. *Find minimum of constrained nonlinear multivariable function*. Feb. 2022. URL: https://www.mathworks.com/help/optim/ug/fmincon.html?searchHighlight=fmincon&s_tid=srchtitle_fmincon_1.
- [19] Thomas Stiehl et al. “Clonal selection and therapy resistance in acute leukaemias: mathematical modelling explains different proliferation patterns at diagnosis and relapse”. In: *Journal of The Royal Society Interface* 11.94 (2014), p. 20140079. DOI: 10.1098/rsif.2014.0079. URL: <https://royalsocietypublishing.org/doi/abs/10.1098/rsif.2014.0079>.

- [20] Stiehl, T. and Marciniak-Czochra, A. “Mathematical Modeling of Leukemogenesis and Cancer Stem Cell Dynamics”. In: *Math. Model. Nat. Phenom.* 7.1 (2012), pp. 166–202. DOI: 10.1051/mmnp/20127199. URL: <https://doi.org/10.1051/mmnp/20127199>.
- [21] Nariaki Sugiura. “Further analysts of the data by akaike’ s information criterion and the finite corrections”. In: *Communications in Statistics - Theory and Methods* 7.1 (1978), pp. 13–26. DOI: 10.1080/03610927808827599. URL: <https://doi.org/10.1080/03610927808827599>.
- [22] Frederik Ziebell, Ana Martin-Villalba, and Anna Marciniak-Czochra. “Mathematical modelling of adult hippocampal neurogenesis: effects of altered stem cell dynamics on cell counts and bromodeoxyuridine-labelled cells”. In: *Journal of The Royal Society Interface* 11.94 (2014), p. 20140144. DOI: 10.1098/rsif.2014.0144. URL: <https://royalsocietypublishing.org/doi/abs/10.1098/rsif.2014.0144>.
- [23] Frederik Ziebell et al. “Revealing age-related changes of adult hippocampal neurogenesis using mathematical models”. In: *Development* 145.1 (Jan. 2018). dev153544. ISSN: 0950-1991. DOI: 10.1242/dev.153544. eprint: <https://journals.biologists.com/dev/article-pdf/145/1/dev153544/1852642/dev153544.pdf>. URL: <https://doi.org/10.1242/dev.153544>.

Erklärung zur Bachelorarbeit Mathematik mit einem Fachanteil von 100%

Name: Stickel

Vorname: Maria Anita

Matrikelnummer: 4040125

Geburtsdatum: 13.02.1997

Erklärung

Ich bin eingeschriebener Student und habe den Prüfungsanspruch im Bachelorstudiengang oder einem Studiengang mit vergleichbarem Inhalt nicht verloren.

Ich habe die Orientierungsprüfung bestanden und Studienleistungen im Umfang von 120 Leistungspunkten absolviert.

Hiermit versichere ich, dass ich die vorliegende Arbeit selbstständig verfasst habe und dass keine anderen als die angegebenen Quellen und Hilfsmittel benutzt wurden.

Weiterhin erkläre ich, dass diese Arbeit bisher keinem anderen Prüfungsamt in gleicher oder vergleichbarer Form vorgelegt und bisher nicht veröffentlicht wurde.

Heidelberg, den 02.03.2022

M. Stickel